Revealing the Impact of Heat Generation Using Nanographene-Based Light-Emitting Electrochemical Cells

Elisa Fresta, Jacopo Dosso, Juan Cabanillas-Gonzalez, Davide Bonifazi, and Rubén D. Costa*

ABSTRACT: Self-heating in light-emitting electrochemical cells (LECs) has been long overlooked, while it has a significant impact on (i) device chromaticity by changing the electroluminescent band shape, (ii) device efficiency because of thermal quenching and exciton dissociation reducing the external quantum efficiency (EQE), and (iii) device stability because of thermal degradation of excitons and eliminate doped species, phase separation, and collapse of the intrinsic emitting zone. Herein, we reveal, for the first time, a direct relationship between self-heating and the early changes in the device chromaticity as well as the magnitude of the error comparing theoretical/experimental EQEs—that is, an overestimation error of *ca.* 35% at usual pixel working temperatures of around 50 °C. This has been realized in LECs using a benchmark nanographene—that is, a substituted hexa-peri-hexabenzocoronene—as an emerging class of emitters with outstanding device performance compared to the prior art of small-molecule LECs—for example, luminances of 345 cd/m^2 and EQEs of 0.35%. As such, this work is a fundamental contribution highlighting how self-heating is a critical limitation toward the optimization and wide use of LECs.

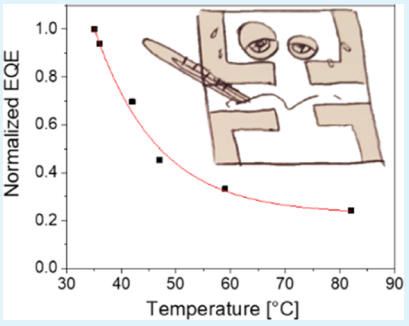

KEYWORDS: *small molecules, nanographenes, self-heating, light-emitting electrochemical cells, device efficiency*

1. INTRODUCTION

Light-emitting electrochemical cells (LECs) are simple and low-cost solid-state emissive devices that consist of a thin-film active layer sandwiched between two air-stable electrodes.[1,2] The active layer comprises a blend of mobile ions and an electroactive emitter. The presence of mobile ions leads to a peculiar working mechanism, in which charge injection and carrier transport depend on ion arrangements under operating conditions. This also allows us to easily fabricate devices with a good tolerance toward the active layer thickness, the type of electrodes/substrates, and the type of deposition techniques. Indeed, LECs could be applied to a myriad of lighting applications, including labeling, decorative, and medical applications, among others.[3−5] However, their wide implementation must also take into account not only a simple device architecture and a low-cost solvent-based fabrication process[5,6] but also an excellent self-stability upon storage and mechanical stress[7] and the right operating conditions to meet the performance criteria for each application.[3,7−15]

In this context, the effect of the temperature on the LEC performance is a critical aspect that has barely been considered in the literature until date.[16−18] In brief, Friend *et al.* reported on the reversible color changes in LECs based on copper(I) complexes upon externally applying temperature,[16] while Slinker and co-workers nicely studied the relationship between the thermal stability of LECs with iridium(III) and ruthenium(II) complexes and the presence of their degradative metal-centered excited states.[17] Finally, Gao and collaborators stated that poor thermally conductive substrates, such as glass, have a dramatic effect on both electroluminescence and driving voltage that can only be explained by the effect of self-heating.[9] In a following contribution, they abruptly cooled the devices to −73 °C, thereby freezing the p−i−n junction and allowing for the study of a static doping profile.[19] We have also described how gentle thermal drying under different atmospheres significantly changes the film morphology, affecting the photoluminescence, electrical, and ion conductivity features in LECs with small molecules and d^{10}-complexes as emitters.[18,20−24]

Much less considered is the impact of the self-heating in LECs caused by the operating conditions.[25] Similar to other thin-film organic/inorganic lighting diodes,[26] the instantaneous heat generation upon driving is related to (i) the resistances associated to the interfaces and the bulk of the active layer (Joule effect) and (ii) the nonradiative deactivation process of excitons (formation of dark/quenched excitons and self-absorption). In LECs, self-heating might also be a source of emitter degradation, exciton dissociation, quick collapse of the intrinsic emitting zone, and morphological changes because the

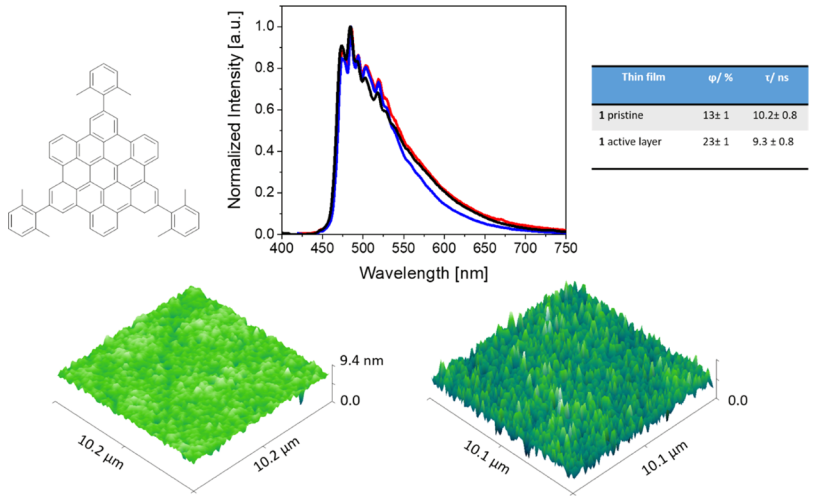

Figure 1. Top: Chemical structure of **1** (left), photoluminescence spectra (centre) of **1** films without (black) and with (blue) a polymer electrolyte, and without ionic polyelectrolyte at 77 K (red) and a table summarizing the photophysical properties of the abovementioned **1** films (right). Bottom: AFM images of **1** films without (right) and with (left) eliminated polymer electrolyte.

internal temperature of the devices can reach values close to 80 °C.[18] Furthermore, the increase in the temperature has a direct impact on (i) the device chromaticity as the emission band shape is broadened because of radiative decay from upper vibrational modes and (ii) the reduction of the external quantum efficiency (EQE) because of the typical thermal quenching leading to decreased photoluminescence quantum yields (ϕ) of the active layer.

As an example for the former, we have recently deciphered the origin of efficient and stable white LECs based on blue-emitting BN-doped nanographenes.[18] We described how the spontaneous heat generation, which led to pixel temperatures of *ca.* 80 °C, activates a ternary radiative mechanism, leading to efficient white photo- and electroluminescence responses. Thus, self-heating must be considered a synergistic effect to others, such as unbalanced doping and movement of the emitting p−i−n region,[27] as well as microcavity and scattering effects,[28−31] for the changes of the electroluminescence spectrum before the operation steady-state regime is reached. Concerning the device efficiency, theoretical EQE values are regularly calculated with ϕ values obtained at room temperature. Because the device temperature can reach values of up to 80 °C,[18] a significant error with respect to the experimental EQE is committed. Thus, the pixel temperature should also be considered upon optimizing the device performance with respect to layer thickness, substrates, driving modes, and so forth. Overall, a full understanding of the temperature influence on the electroluminescence response in LECs would help to focus efforts toward realizing improved emitters and smart device architectures to meet highly efficient and stable devices. In particular, this aspect must be of utmost relevance toward designing lighting devices for medical applications and labeling, as heat dissipation architectures have not been implemented in LECs yet.

Along these lines, the major thrust of this work is the unveiling of the impact of the self-heating on the chromaticity and efficiency of LECs using a benchmark nanographene—that is, hexa-peri-hexabenzocoronene or **1**[32]—as an emerging class of emitters with outstanding device performance. Because LECs show a high versatility with respect to the type of emitters,[4,23,33−39] the impact of self-heating can, indeed, be considered as universal. For instance, Figure S1 displays the working pixel temperature of 40−50 °C LECs with d^6-/d^{10}-complexes and small molecules operating at pulsed 100 mA/cm^2,[7,24,40] while Edman's group has recently showed that polymer-LECs reach 50 °C at 50 mA/cm^2.[25] Our interest on nanographenes lies on their high ϕ, ambipolar carrier properties, sound thermal and redox stabilities, and a good solubility in common organic solvents.[32,41,42] Despite these appealing properties, they have barely been investigated as emitters in thin-film lighting devices.[41] In stark contrast, we have recently reported highly stable and efficient red-emitting LECs with contorted nanographenes[24] and highly efficient white-emitting LECs with B−N-doped nanographenes—*vide supra*.[18] In this line, **1**-LECs show one of the best-performing green-emitting LECs based on small-molecule emitters regardless of the chosen driving mode—for example, maximum luminances of 345 cd/m^2 and EQEs of 0.35%.[4] Finally, the electroluminescent behavior of **1**-LECs allowed us to contextualize clear relationships between self-heating and the early changes of the electroluminescence spectra as well as the source and magnitude of the error in the experimental/theoretical EQE calculations, accounting for values of up to 35% depending on the driving modes and pixel temperatures.

Overall, this work states the relevance of self-heating as a critical limitation in the optimization of both, device performance (color and efficiency) and device application (medicine, labeling, *etc.*), regardless of the type of the emitter.

2. RESULTS AND DISCUSSION

The synthesis and photophysical characterization of **1** in solution was reported elsewhere,[32] showing blue-green fluorescence and yellow-orange phosphorescence at room temperature and 77 K, respectively—as shown in Figure S2. We have further prepared thin films with only **1** and with blends of **1** with the polymer electrolyte mixture used in devices—that is, **1**/PS/PEO/LiOTf in a mass ratio 10:0.9:2.6:0.78, being PS (polystyrene), PEO (polyethylene oxide), and LiOTf (lithium triflate); see the Supporting Information for more details. Atomic force microscopy (AFM) assays confirm that both films show a similar homogeneous morphology with a root-mean-square roughness of around 2

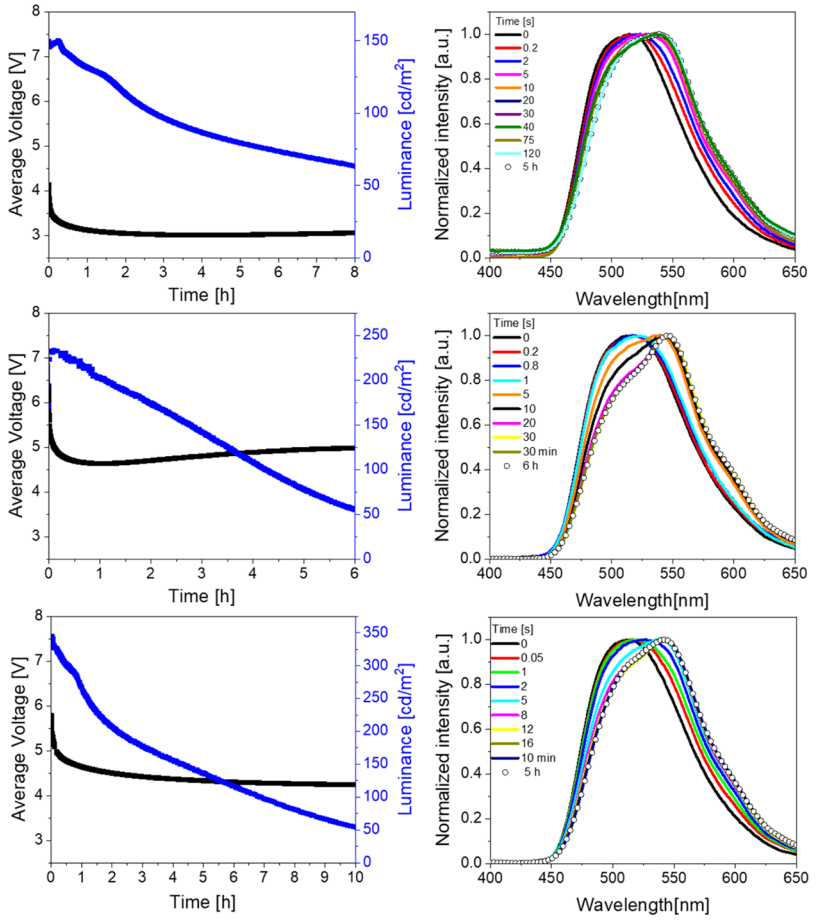

Figure 2. Average voltage and luminance *vs* time (left) and selected electroluminescence bands over time (right) of **1**-LECs driven at pulsed currents of 15 (top), 25 (center), and 55 (bottom) mA.

Table 1. Figures of Merit of 1-LECs Driven at Pulsed Current and Constant Voltage

driving mode [mA]	luminance [cd/m^2]	t_{on}[c] [min]	$t_{1/2}$[d] [h]	E_{tot}[e] [J]	efficiency [cd/A]	EQE[f] [%]	*x*/*y* CIE color coordinates (fresh-final)
15 mA[a]	157 ± 13	0.48 ± 0.03	5.8 ± 0.6	483 ± 51	0.20 ± 0.02	$8.6 \times 10^{-2} \pm 1.1 \times 10^{-2}$	0.31–0.37/0.49–0.52
25 mA[a]	233 ± 21	0.24 ± 0.02	3.8 ± 0.3	469 ± 49	0.18 ± 0.02	$2.5 \times 10^{-2} \pm 2.7 \times 10^{-3}$	0.31–0.38/0.49–0.52
55 mA[a]	343 ± 28	0.18 ± 0.02	3.0 ± 0.2	545 ± 56	0.12 ± 0.01	$7.2 \times 10^{-3} \pm 9 \times 10^{-4}$	0.31–0.36/0.49–0.54
3.5 V[b]	12 ± 2	12.0 ± 0.01	5.5 ± 0.6	35 ± 4	0.12 ± 0.01	$3.5 \times 10^{-1} \pm 3.8 \times 10^{-2}$	0.29–0.32/0.44–0.44
4.5 V[b]	36 ± 4	3.1 ± 0.03	0.23 ± 0.2	4.4 ± 0.5	0.20 ± 0.02	$1.9 \times 10^{-1} \pm 2.2 \times 10^{-2}$	0.30–0.33/0.44–0.46
6 V[b]	133 ± 14	0.60 ± 0.05	0.17 ± 0.02	12 ± 0.1	0.11 ± 0.01	$1.3 \times 10^{-2} \pm 1.7 \times 10^{-3}$	0.30–0.34/0.44–0.53

[a]Pulsed mode. [b]Constant mode. [c]Turn on time: time to reach the maximum luminance. [d]Lifetime: time to reach 50% of the maximum luminance. [e]Total emitted energy: calculated from integration of the radiant flux of the device *vs* time from $t = 0$ (application of bias) to $t = t_{1/5}$. [f]External quantum efficiency: ratio of emitted photons per injected electrons.

nm—as shown in Figure 1. Similar to the photoluminescence in solution, both films exhibit a well-structured emission centered at *ca.* 500 nm with associated ϕ values of 23 and 14% with and without a polymer electrolyte, respectively—as shown in Figure 1, while it is very interesting to note the lack of phosphorescence in thin films at 77 K.

To study the electroluminescence behavior of **1**, a series of devices with the architecture ITO/PEDOT:PSS (70 nm)/**1**/PS/PEO/LiOTf (10:0.9:2.6:0.78; 70 nm)/Al were prepared—see the Supporting Information for more details. Here, this polymer electrolyte mixture was already proposed by Edman and co-workers to avoid phase separation upon film forming and over time.[43] Indeed, it was selected as other commonly used matrices [*i.e.*, trimethylol propane ethoxylate (TMPE)/LiOTf] led to phase separation upon device fabrication. These devices were driven at a pulsed current of 15, 25, and 55 mA, monitoring luminance, color, and electrical features over time—as shown in Figure 2 and Table 1. Regardless of the applied current, they exhibited the typical LEC behavior with a high initial average voltage that exponentially reduces, reaching a plateau close to the energy band gap of **1**. This goes hand-in-hand with an initial increase in the luminance toward its maximum value that then slowly decreases, realizing stabilities—that is, lifetime/total emitted energy—of 5.8 h/483 J, 3.8 h/469 J, and 3 h/545 J for 15, 25, and 55 mA, respectively. Finally, the device efficiency linearly decreases from 0.20, 0.18, and 0.12 cd/A upon increasing the applied current. Contextualizing the abovementioned device performance, **1**-LECs stand among the best in the prior art of green-emitting small-molecule LECs.[44−47]

Interesting are the changes in the electroluminescence spectra under operation—as shown in Figure 2. At the very early stage, a broad emission band with a slightly red-shifted maximum peak that is associated to a green emission—that is, λ_{max} = 510 nm; x/y CIE color coordinates of 0.31/0.49—was noted at any applied current—as shown in Figures 2 and 3.

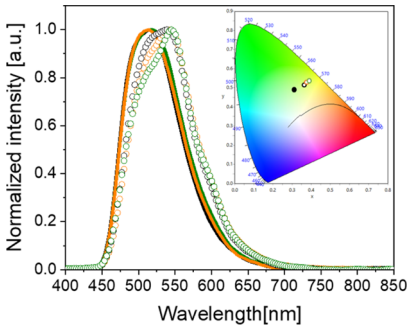

Figure 3. Electroluminescence emission bands and their respective x/y CIE color coordinates (inset) of fresh (solid) and after 1 h of driving (open) **1**-LECs driven at 15 (black), 25 (orange), and 55 (green) mA.

The differences between the photo- and electroluminescence responses might be attributed to the electric polarization effect that modifies the radiative vibrational deactivation rates and provokes the stabilization of the excited state.[48] However, the electroluminescence band quickly sharpens—as shown in Figure 2, featuring a final structured yellowish green emission—that is, λ_{max} at 545 nm with a shoulder at 505 nm; x/y CIE color coordinates of 0.34/0.50, as shown in Figure 3. Interestingly, the time to reach a stable electroluminescence spectrum depends on the applied current. For instance, Figure 2 shows that the electroluminescence spectrum stabilizes after 120 s, 30 s, and 8 s for devices driven at 15, 25, and 55 mA, respectively. Common to all the devices, the electroluminescence energy onset of the band and the full width at half-maximum values of the electroluminescence spectra hold constant at *ca.* 2.75 eV and *ca.* 95 nm, pointing out that the same excited state is responsible for the initial and final emission features. At this point, we can discard the contribution of triplet excited states to the electroluminescence. On the one hand, phosphorescence was not observed at 77 K in thin films—as shown in Figure 1. On the other hand, electroluminescence and phosphorescence from frozen solutions are clearly dissimilar; the latter consists of a band centered at λ_{max} at 580 nm with shoulders at 630 and 680 nm—as shown in Figure S2.

Because observed electroluminescence changes rapidly occur before the electrical steady-state regime of the device is reached and hold over the lifespan of the devices, we ruled out effects related to (i) variations in the internal local electric field distribution[24,49−52] and (ii) microcavity effects due to the movement of the emitting p−i−n region.[27] In addition, the formation of emitting degradative species was also discarded using spectroscopic techniques. In short, static electrochemical impedance spectroscopy (EIS) measurements—that is, the frequency scan at increasing applied voltages from 0 to 5 V, as shown in Figures 4, S3, and S4—of fresh devices show a common LEC behavior: (i) an initial decrease in the resistance at biases below the energy band gap (*ca.* 3.0 V), indicating the formation of electrical double layers at the electrode interfaces, and (ii) a further resistance decrease that holds at higher

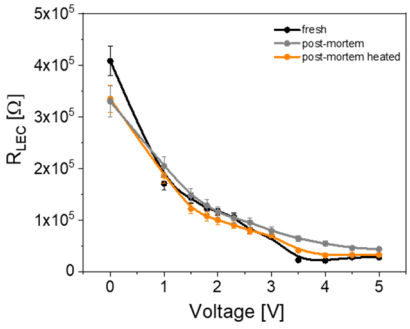

Figure 4. Resistance values *vs* applied voltage of fresh, used (pulsed 25 mA), and heated (60 °C for 1 h) **1**-LECs.

biases, which accounts for the formation of the doped regions and the autosustained charge recombination.[7,24,39,53−55] In contrast, used devices have been polarized, featuring slightly decreased resistance values than fresh devices and a linear decrease in the resistance upon biasing from 0 to 5 V. By heating them at 60 °C for 1 h, the polarization induced by previous biasing is erased and the resistance *versus* applied voltage resembles that of fresh devices with a clear drop at *ca.* 3.5−4 V. Here, the slightly higher resistance observed above the threshold voltage in used devices may suggest slight degradation. However, the absorption and emission features of fresh and used devices are similar—as shown in Figure S5. Therefore, we discard degradation as the responsible for the change in electroluminescence over time.

Next, the electroluminescence behavior is put into context with the direct comparison with the photoluminescence of the films. The PL spectrum features a rich vibrational structure covering a spectral range from 476 to 590 nm—as shown in Figures 1 and 5. As a matter of fact, the vibrational structure

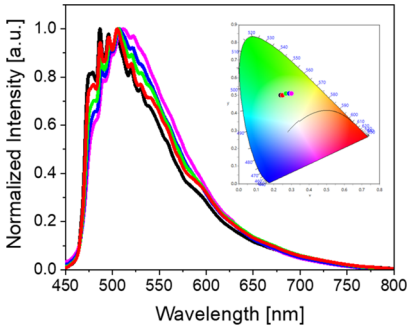

Figure 5. Photoluminescence spectra (λ_{exc} = 405 nm) of **1** thin films with the same composition as **1**-LECs upon heating at rt (black), 50 °C (red), 100 °C (green), 150 °C (blue), and 200 °C (magenta), with their respective x/y CIE coordinates (inset).

can easily be altered applying heat or electric fields. To shed light onto temperature-dependent emission, we studied the photoluminescence of **1**-films with the same composition as **1**-LECs under vacuum upon increasing temperature from rt to 200 °C—as shown in Figure 5. Uncommonly, the emission intensity is fivefold increased at high temperatures. This is corroborated by the improvement of ϕ upon increasing the temperature—as shown in Figure S6. The reasons leading to this rare increase are not fully understood yet. This could be related to a reduced vibrational exchange energy between singlet excited states or temperature-induced short-range morphological changes in the films, reducing intermolecular

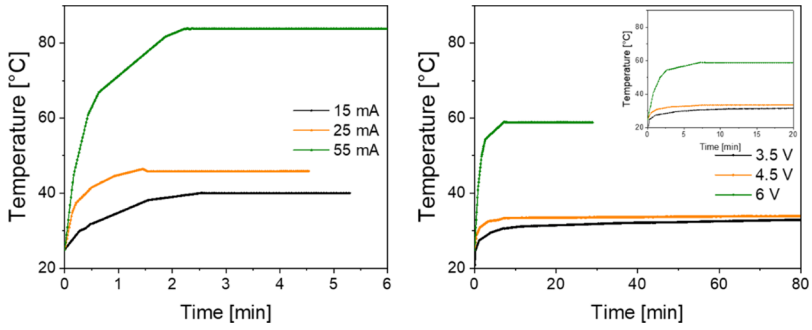

Figure 6. Temperature rise in **1**-LECs using pulsed currents (left) and constant voltage (right). Inset: zoom on the first 20 min of measurement. The error in the temperature measurement is of ±2 °C.

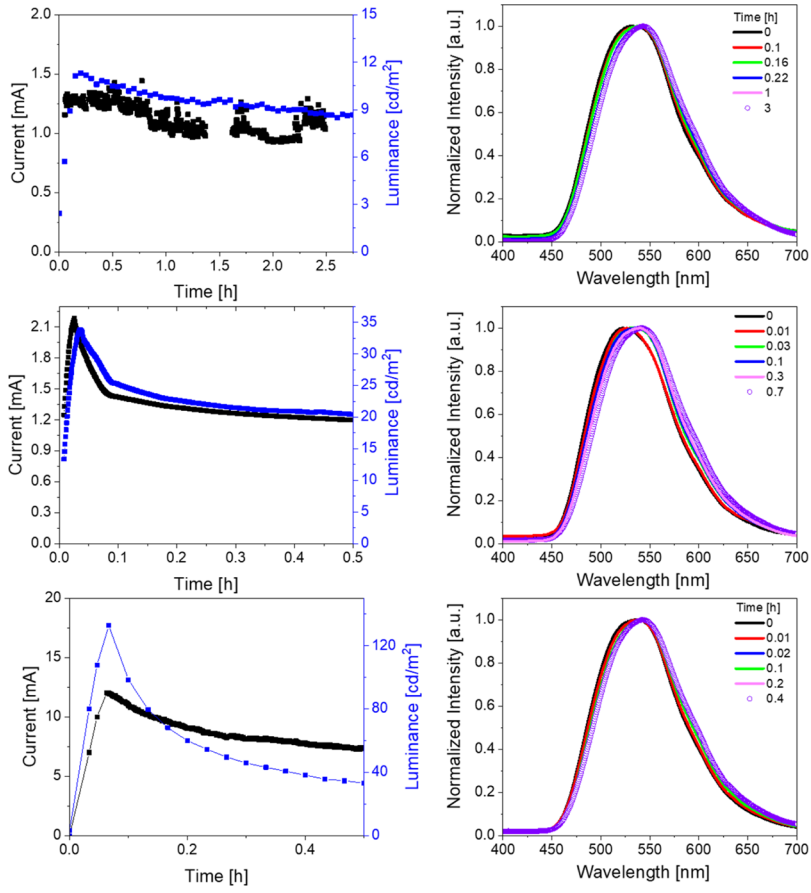

Figure 7. Current and luminance *vs* time (left) and selected electroluminescence bands over time (right) of **1**-LECs driven at a constant voltage of 3.5 (top), 4.5 (center), and 6.5 (bottom) V.

interactions like aggregates.[56,57] As far as the emission band shape is concerned, the high-energy vibrational features (λ < 500 nm) decrease, while the low-energy vibrational peaks (λ > 530 nm) are enhanced upon increasing the temperature. This leads to a color emission change from blue to yellow–green that resembles those in the devices. Finally, the τ (λ_{exc} = 405 nm) values at 486 and 600 nm upon heating were similar in the nanosecond regime—as shown in Table S1, corroborating the exclusive presence of fluorescence on the overall emission.

In view of the above-described results, the reason underlying the electroluminescence changes might imply (i) the modification of the radiative deactivation rate of excited vibrational states promoted by the synergistic effect of the external electric field and the increased pixel temperature and (ii) doping-induced self-absorption.[58] Regarding the first point, the pixel temperature might be considered as the dominant process because the average voltage showed a similar slow decay and plateau—as shown in Figure 2, indicating that the applied electric field distribution across the active layer might follow a similar evolution. As for the second point, self-absorbing species would cause a continuous variation in the electroluminescence response, which, however, does not change relevantly after, on average, minutes of measurement. In addition, the temperature-dependent photoluminescence shows the same behavior as the electroluminescence, while self-absorption does not apply here.

Further corroboration comes from the correlation between the increase in the pixel temperature and the spectral changes

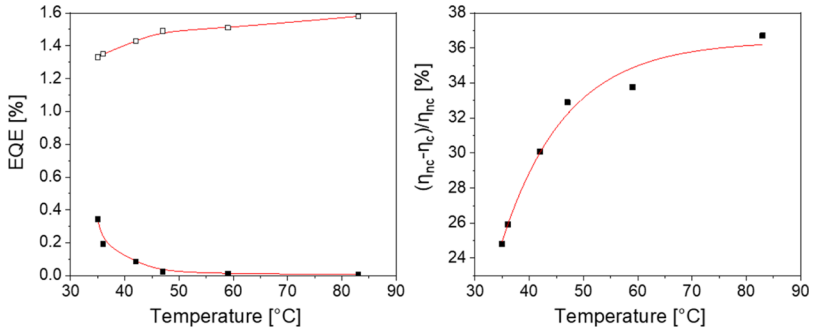

Figure 8. Left: Experimental (solid symbol) and theoretical (open symbol) EQE values *vs* pixel working temperature of **1**-LECs operating at pulsed current and constant voltage driving modes. Right: Error *vs* pixel working temperature of **1**-LECs operating at pulsed current and constant voltage driving modes. The red lines display the fittings. The fitting models are presented in the Supporting Information.

using different driving conditions. In particular, operating at pulsed 15 mA leads to an exponential increase in temperature up to 40 °C during the first 2 min—as shown in Figure 6, holding constant over time. The increase in the current compliance leads to both, a quicker heat generation—for example, 40 °C is reached at 24 s (25 mA) and 7 s (55 mA)—and higher maximum temperature values of *ca.* 50 °C (25 mA) and 90 °C (55 mA). The increase in the pixel temperature nicely fits with the time to stabilize the electroluminescence response under the pulsed driving mode—that is, 2 min, 20 s, and 8 s, for 15, 25, and 55 mA, respectively, as shown in Figure 2. Noteworthy, the temperature rise profile is similar to that commented by Edman and co-workers.[25]

Finally, we also analyzed devices driven at constant applied voltage—that is, 3.5, 4.5, and 6 V, as shown in Figure 7 and Table 1. In line with the literature,[8] these devices exhibited similar efficiencies and lower luminance and stability values compared to those driven at pulsed current—as shown in Table 1. Likewise, all the devices show (i) the same initial green and broad electroluminescence spectrum—that is, λ_{max} = 520 nm; x/y CIE color coordinates of 0.29/0.44—independent of the driving voltage and (ii) a slow change until a stable yellowish green electroluminescence band is reached—that is, λ_{max} = 548 nm; x/y CIE color coordinates of 0.44/0.53. The time to reach a stable emission band decreases from 32 to 13.2 and to 7.2 min for devices driven at 3.5, 4.5, and 6 V, respectively. This behavior corresponds to the time to reach the plateau temperature observed in devices, that is, 30 min (3.5 V), 12 min (4.5 V), and 8 min (6 V).—as shown in Figure 6. The highest temperature values of 35, 36, and 59 °C are reached for 3.5, 4.5, and 6 V, respectively—as shown in Figure 6. This might be related to the reduced density of the injected carrier compared to the pulsed driving mode—for example, 12.5 mA at 6 V.

As mentioned above, **1** shows a peculiar enhancement of the ϕ values with the temperature—see the Experimental Section, Figure S6, and Table S2 for details. Taking the ϕ of *ca.* 23% at 25 °C as the reference, this figure exponentially increases up to 37% at 83 °C—as shown in Figure S6. This must be translated into an increase in the fraction of excitons that decay radiatively (φ) under operating conditions. In **1**-LECs, the maximum φ is 1/4 of ϕ in thin films, as, statistically, 1/4 of the electron–hole recombination produces singlets. Thus, the EQE, which is defined as EQE = $b\varphi/2n^2$, where b is the recombination efficiency (equal to 1 for two ohmic contacts) and n is the refractive index of the glass substrate and is equal to 1.5 (the factor $1/2n^2$ represents the light out-coupling of the device, while we assume that the change in refractive index with temperature is negligible), is also temperature-dependent and must be calculated taking into account the temperature dependence of ϕ with respect to the pixel temperature under operation. For instance, after gathering all the abovementioned devices measured at different driving modes, as ϕ increases with the temperature, the theoretical EQE increases from 1.28% (rt) to 1.58% (83 °C), in a manner that can be described using a Gompertz growth model—as shown in Figure 8 and Table S3, while the experimental value decreases with the working temperature in a manner that is well-described using a $y = 1/(x + A)$ function—as shown in Figure 8 and Table S4.

The ratio between experimental and theoretical EQE values (η = EQE_{exp}/EQE_{theo}) is typically used to determine the optimization degree of the devices using different driving modes. At pulsed currents of 15, 25, and 55 mA, η values are 0.067, 0.019, and 0.0057 considering ϕ at 25 °C, while η values of 0.047, 0.013, and 0.0036 are recalculated taking into account the pixel working temperature. Likewise, devices driven at a constant bias of 3.5, 4.5, and 6 V show a η value of 0.27, 0.15, and 0.010 and 0.20, 0.11, and 0.0067 with and without considering pixel temperature, respectively. We can contextualize all these results calculating the % error—that is, $((\eta_{nc}-\eta_c)/\eta_{nc}) \times 100$—between the uncorrected (η_{nc}) and corrected (η_c) values with the temperature, regardless of the driving mode—as shown in Tables S5 and S6 and Figure 8. Thus, the error *versus* pixel temperature obeys an exponential rise similar to that of $\phi(T)$, accounting for an overestimation error of *ca.* 35% at usual working temperatures (50 °C) that has been long neglected. This simple analysis testifies that self-heating is critical for the optimization of devices driven at pulsed modes as high working temperatures of 40–60 °C are typically reached—as shown in Figure S1. In contrast, the optimization using a constant voltage driving mode seems to be more reliable as long as carrier density is low.

3. CONCLUSIONS

This work provides the first comprehensive study about the impact of the self-heating on the device chromaticity and efficiency in LECs. To this end, we have focused on a benchmark nanographene as an emerging class of emitters that lead to outstanding device performances (luminance of 345 cd/m^2 and EQE of 0.35%) compared to the prior art in small-molecule-based LECs. The relevance of this work lies on two important findings. On the one hand, a direct relationship between the rise of the pixel temperature (self-heating) and the

changes of the device electroluminescence band shape over time is provided. Thus, a rationale about early chromaticity changes in LECs might also include the heat generation under operating conditions, as a synergistic parameter to others related to optical and electrical phenomena. On the other hand, a source and magnitude of the error upon optimizing the device with respect to η as the ratio theoretical/experimental EQE is highlighted. As a matter of fact, ϕ values are temperature-dependent and, in turn, the theoretical EQE must be also recalculated taking into account the pixel temperature. Regardless of the driving mode, we have estimated errors of up to *ca.* 35% at usual working temperatures of 40−50 °C in nanographene LECs.

Overall, this work represents a key contribution, highlighting how self-heating is a critical parameter that must be taken into consideration toward (i) rationalizing the design of emitters and device architectures to optimize device performance (color and efficiency) and (ii) engineering of smart devices for applications in medicine and labeling applications, among others.

4. EXPERIMENTAL SECTION

4.1. Materials. All chemicals were purchased from chemical suppliers and used without further purification. All analytical reagent-grade solvents were purified by distillation. All reactions were carried out under an inert nitrogen atmosphere using standard vacuum line techniques.

4.2. Synthesis and Spectroscopic, Electrochemical, and Microscopy Characterization. **1** was synthesized as reported in a previous contribution.[32] Absorption spectra were recorded with a PerkinElmer Lambda 35 ultraviolet (UV)−vis spectrometer. The photoluminescence spectra and ϕ values at 25 °C were measured with an FS5 Spectrofluorometer with an integrating sphere SC-30 (Edinburgh Instruments). Photoluminescence measurements at temperatures ranging from 25 to 202 °C were performed upon enclosing HBC films in a CFV-Optistat (Oxford Instruments) equipped with a temperature controller. Films were photoexcited with a TEEM Photonics passive Q-switch Nd:YAG laser (405 nm, 300 ps pulse duration, 170 Hz, pulse energy < 1 mJ) mildly focused on the sample (fluence < 10 mJ/cm^2). The photoluminescence emitted by the samples was dispersed using a grating inside a spectrometer (SP2500, Acton Research) and spectrally recorded with a liquid N_2-cooled back-depleted CCD (Princeton Instruments). Long-pass filters were employed to reject stray light from the photoexcitation beam into the spectrometer. The photoluminescence spectra were acquired 10 min after the sample reached the desired temperature in order to ensure complete sample thermalization. The temperature dependence of the ϕ values by recalculating considering the differences in the integration of the absorption and emission spectra at different temperatures with respect to that measured at rt. Excited state lifetimes (τ) were obtained with a time-correlated single-photon counting (TCSPC) with λ_{exc} = 405 nm and the corresponding exponential fitting: $R(t) = \sum_{i=1}^{2} A_i e^{-t/\tau_i}$. The average lifetime values $\langle\tau\rangle$ were obtained with: $\langle\tau\rangle = \frac{A_1\tau_1^2 + A_2\tau_2^2 + A_3\tau_3^2}{A_1\tau_1 + A_2\tau_2 + A_3\tau_3}$.

Device and film temperature was obtained using an FLIR-430sc thermal camera and the absorption scan was performed in 30 s to avoid excessive cooling. Thin films (75 nm) were prepared onto cleaned quartz slides from a filtered solution of **1** (10 mg/mL in THF; without or with an ion-doped matrix, as below described) using a spin-coated matrix at 800 rpm for 30 s, at 1500 rpm for 30 s, and at 3000 rpm for an additional 10 s. AFM measurements were carried out with a Park XE150 instrument (Park Systems Corp., Suwon, South Korea) and the Gwyddion evaluation software.

4.3. Device Fabrication and Characterization. Indium−tin oxide (ITO) substrates were purchased from Naranjo Substrates with an ITO thickness of 130 nm. They were extensively cleaned using detergent, water, ethanol, and propan-2-ol as solvents in an ultrasonic bath (frequency 37−70 Hz) for 15 min each. Afterward, the slides were dried with N_2 gas and put in a UV−ozone cleaner for 8 min and used directly as described in the main text. As PEDOT:PSS was used to increase reproducibility, the clean plates were coated with 70 nm PEDOT:PSS layers *via* spin-coating. To this end, an aqueous solution of PEDOT:PSS was filtered and mixed with propan-2-ol in a ratio of 3:1. From this solution, 50 μL was dropped onto the substrate at a rotation speed of 2000 rpm and spun for 60 s. The resulting layers were dried on a hotplate at 120 °C and stored under N_2. Thick active layers (100 nm) were deposited from 10 mg/mL **1** combined with a ion-doped matrix consisting of **1**/PS/PEO/LiOTf 10:1.81:2.6:0.78 mass ratio. This was prepared using THF solutions of PS (polystyrene) with M_w 900,000 (10 mg/mL), PEO (polyethylene oxide) (20 mg/mL), and LiOTf (lithium triflate) (10 mg/mL) and spin-coated at 800 rpm for 30 s, at 1500 rpm for 30 s, and at 3000 rpm for an additional 10 s, resulting in 70 nm of the active layer thickness. In all cases, after the deposition of the active layer, the devices were dried under vacuum for 2 h and transferred to an inert atmosphere glovebox (<0.1 ppm O_2 and H_2O, Angstrom Engineering). Finally, aluminum cathodes (90 nm) were thermally evaporated onto the active layer using a shadow mask under high vacuum (<1 × 10^{-6} mbar) in an Angstrom Covap evaporator integrated into the inert atmosphere glovebox. The device statistics involve up to five different devices—that is, a total number of 20 pixels. Time dependence of luminance, voltage, and current was measured by applying constant and/or pulsed voltage and current by monitoring the desired parameters simultaneously using an Avantes spectrophotometer (Avaspec-ULS2048L-USB2) in conjunction with a calibrated integrated sphere Avasphere 30-Irrad and Botest OLT OLED Lifetime-Test System. Electroluminescence spectra were recorded using the abovementioned spectrophotometer. The temperature of the devices upon driving was recorded with a FLIR 430-sc thermal camera. EIS assays were carried out with a potentiostat/galvanostat (Metrohm μAutolabIII) equipped with a frequency response analyzer module (FRA2). Measurements were performed at the applied voltage range from 0 to 6 V and fitted with the Nova software using the circuit model, as shown in Figure S3. The ac signal amplitude was set to 15 mV and modulated in a frequency range from 10 to 1 MHz. The Nova 1.11 software was used to obtain the parameters from the equivalent circuit. With this data at hand, the resistance of the intrinsic nondoped region (R_{LEC}) was directly obtained. The temperature of the devices upon driving was recorded with a FLIR 430-sc thermal camera.

■ ASSOCIATED CONTENT

Supporting Information

The Supporting Information is available free of charge at https://pubs.acs.org/doi/10.1021/acsami.0c06783.

Thermal pictures of selected LECs, absorption spectrum of **1**, EIS circuits used to fit EIS data, absorption spectrum of 1-LECs (fresh and used), Φ/Φ_{rt} ratio at different temperatures, photoluminescence features of **1**: electrolyte matrix at different temperatures, τ values measured at different temperatures, model and parameters employed to describe EQE-related figures of merit of **1**-LECs, and experimental and theoretical EQE-related figures of merit of **1**-LECs (PDF)

■ AUTHOR INFORMATION

Corresponding Author

Rubén D. Costa − *IMDEA Materials Institute, E-28906 Getafe, Spain;* orcid.org/0000-0003-3776-9158; Email: ruben.costa@imdea.org

Authors

Elisa Fresta − *IMDEA Materials Institute, E-28906 Getafe, Spain; Departamento de Física Aplicada, Universidad Autónoma de Madrid, 28049 Madrid, Spain*

Jacopo Dosso − *School of Chemistry, Cardiff University, CF10 3AT Cardiff, Great Britain*

Juan Cabanillas-Gonzalez − *IMDEA Nanoscience, 28049 Madrid, Spain;* orcid.org/0000-0002-9926-3833

Davide Bonifazi − *School of Chemistry, Cardiff University, CF10 3AT Cardiff, Great Britain; Institute of Organic Chemistry, Faculty of Chemistry, University of Vienna, 1090 Vienna, Austria;* orcid.org/0000-0001-5717-0121

Complete contact information is available at: https://pubs.acs.org/10.1021/acsami.0c06783

Author Contributions

The manuscript was written through contributions of all authors. All authors have given approval to the final version of the manuscript.

Notes

The authors declare no competing financial interest.

■ ACKNOWLEDGMENTS

E.F. and R.D.C. acknowledge the program "Ayudas para la atracción de talento investigador—Modalidad 1 of the Consejería de Educación, Juventud y Deporte—Comunidad de Madrid with reference number 2016-T1/IND-1463". R.D.C. also acknowledges the Spanish MINECO for the Ramon y Cajal program (RYC-2016-20891) and HYNANOSC (RTI2018-099504-A-C22). R.D.C. also acknowledges the FOTOART-CM project funded by the Madrid region under program P2018/NMT-4367. D.B. and J.D. gratefully acknowledge the EU through the MC-RISE project "INFUSION" (734834), MC-ITN project "PHOTOTRAIN" (722591), and Cardiff University for the financial support. J.C.-G. acknowledges financial support from the Spanish Ministry of Science, Innovation and Universities (RTI2018-097508-B-I00) and from the Regional Government of Madrid (S2018/NMT4511). IMDEA Nanociencia acknowledges support from the "Severo Ochoa" Program for Centers of Excellence in R&D (MINECO, grant no. SEV-2016-0686).

■ REFERENCES

(1) Matyba, P.; Maturova, K.; Kemerink, M.; Robinson, N. D.; Edman, L. The Dynamic Organic P-n Junction. *Nat. Mater.* **2009**, *8*, 672−676.

(2) Pei, Q.; Yu, G.; Zhang, C.; Yang, Y.; Heeger, A. J. Polymer Light-Emitting Electrochemical Cells. *Science* **1995**, *269*, 1086−1088.

(3) Costa, R. D. *Light-Emitting Electrochemical Cells. Concepts, Advances and Challenges*, 1st ed.; Springer International Publishing: Basel, 2017.

(4) Fresta, E.; Costa, R. D. Beyond Traditional Light-Emitting Electrochemical Cells-a Review of New Device Designs and Emitters. *J. Mater. Chem. C* **2017**, *5*, 5643−5675.

(5) Tang, S.; Edman, L. Light-Emitting Electrochemical Cells: A Review on Recent Progress. *Top. Curr. Chem.* **2016**, *374*, 40.

(6) Chen, Z.; Li, F.; Zeng, Q.; Yang, K.; Liu, Y.; Su, Z.; Shan, G. Inkjet-Printed Pixelated Light-Emitting Electrochemical Cells Based on Cationic Ir(III) Complexes. *Org. Electron.* **2019**, *69*, 336−342.

(7) Fresta, E.; Monclús, M. A.; Bertz, M.; Ezquerro, C.; Molina-Aldareguia, J. M.; Berenguer, J. R.; Kunimoto, M.; Homma, T.; Costa, R. D. Key Ionic Electrolytes for Highly Self-Stable Light-Emitting Electrochemical Cells Based on Ir(III) Complexes. *Adv. Opt. Mater.* **2020**, 2000295.

(8) Rudmann, H.; Shimada, S.; Rubner, M. F. Solid-State Light-Emitting Devices Based on the Tris-Chelated Devices Based on Derivatives of the Tris (2, 2 ′ -Bipyridyl) Ruthenium (II) Complex. *J. Am. Chem. Soc.* **2002**, *124*, 4918−4921.

(9) Zhang, Y.; Gao, J. Lifetime Study of Polymer Light-Emitting Electrochemical Cells. *J. Appl. Phys.* **2006**, *100*, 084501.

(10) Gao, J. Polymer Light-Emitting Electrochemical Cells—Recent Advances and Future Trends. *Curr. Opin. Electrochem.* **2018**, *7*, 87−94.

(11) Edman, L. Bringing Light to Solid-State Electrolytes: The Polymer Light-Emitting Electrochemical Cell. *Electrochim. Acta* **2005**, *50*, 3878−3885.

(12) Li, X.; Altal, F.; Liu, G.; Gao, J. Long-Term, Intermittent Testing of Sandwich Polymer Light-Emitting Electrochemical Cells. *Appl. Phys. Lett.* **2013**, *103*, 243304.

(13) Slinker, J.; Bernards, D.; Houston, P. L.; Abruña, H. D.; Bernhard, S.; Malliaras, G. G. Solid-State Electroluminescent Devices Based on Transition Metal Complexes. *Chem. Commun.* **2003**, 2392−2399.

(14) AlTal, F.; Gao, J. High Resolution Scanning Optical Imaging of a Frozen Planar Polymer Light-Emitting Electrochemical Cell: An Experimental and Modelling Study. *Sci. China: Chem.* **2017**, *60*, 497−503.

(15) AlTal, F.; Gao, J. High Resolution Scanning Optical Imaging of a Frozen Polymer P-n Junction. *J. Appl. Phys.* **2016**, *120*, 115501.

(16) Asil, D.; Foster, J. A.; Patra, A.; de Hatten, X.; del Barrio, J.; Scherman, O. A.; Nitschke, J. R.; Friend, R. H. Temperature- and Voltage-Induced Ligand Rearrangement of a Dynamic Electroluminescent Metallopolymer. *Angew. Chem., Int. Ed.* **2014**, *53*, 8388−8391.

(17) Bowler, M. H.; Guo, T.; Bastatas, L. D.; Moore, M. D.; Malko, A. V.; Slinker, J. D. Understanding the Superior Temperature Stability of Iridium Light-Emitting Electrochemical Cells. *Mater. Horiz.* **2017**, *4*, 657−664.

(18) Fresta, E.; Dosso, J.; Cabanillas-González, J.; Bonifazi, D.; Costa, R. D. Origin of the Exclusive Ternary Electroluminescent Behavior of BN-Doped Nanographenes in Efficient Single-Component White Light-Emitting Electrochemical Cells. *Adv. Funct. Mater.* **2020**, 1906830.

(19) AlTal, F.; Gao, J. Scanning Photocurrent and PL Imaging of a Frozen Polymer P-i-n Junction. *Phys. Status Solidi RRL* **2015**, *9*, 77−81.

(20) Puscher, B. M. D.; Aygüler, M. F.; Docampo, P.; Costa, R. D. Unveiling the Dynamic Processes in Hybrid Lead Bromide Perovskite Nanoparticle Thin Film Devices. *Adv. Energy Mater.* **2017**, *7*, 1602283.

(21) Weber, M. D.; Garino, C.; Volpi, G.; Casamassa, E.; Milanesio, M.; Barolo, C.; Costa, R. D. Origin of a Counterintuitive Yellow Light-Emitting Electrochemical Cell Based on a Blue-Emitting Heteroleptic Copper(I) Complex. *Dalton Trans.* **2016**, *45*, 8984−8993.

(22) Weber, M. D.; Wittmann, J. E.; Burger, A.; Malcıoğlu, O. B.; Segarra-Martí, J.; Hirsch, A.; Coto, P. B.; Bockstedte, M.; Costa, R. D. From White to Red: Electric-Field Dependent Chromaticity of Light-Emitting Electrochemical Cells Based on Archetypal Porphyrins. *Adv. Funct. Mater.* **2016**, *26*, 6737−6750.

(23) Fresta, E.; Weber, M. D.; Fernandez-Cestau, J.; Costa, R. D. White Light-Emitting Electrochemical Cells Based on Deep-Red Cu(I) Complexes. *Adv. Opt. Mater.* **2019**, *7*, 1900830.

(24) Fresta, E.; Baumgärtner, K.; Cabanillas-Gonzalez, J.; Mastalerz, M.; Costa, R. D. Bright, Stable, and Efficient Red Light-Emitting Electrochemical Cells Using Contorted Nanographenes. *Nanoscale Horiz.* **2020**, *5*, 473−480.

(25) Ràfols-Ribé, J.; Robinson, N. D.; Larsen, C.; Tang, S.; Top, M.; Sandström, A.; Edman, L. Self-Heating in Light-Emitting Electrochemical Cells. *Adv. Funct. Mater.* **2020**, 1908649.

(26) Tyagi, P.; Srivastava, R.; Giri, L. I.; Tuli, S.; Lee, C. Degradation of Organic Light Emitting Diode: Heat Related Issues and Solutions. *Synth. Met.* **2016**, *216*, 40−50.

(27) Tang, S.; Sandström, A.; Lundberg, P.; Lanz, T.; Larsen, C.; Van Reenen, S.; Kemerink, M.; Edman, L. Design Rules for Light-Emitting Electrochemical Cells Delivering Bright Luminance at 27.5 Percent External Quantum Efficiency. *Nat. Commun.* **2017**, *8*, 1190.
(28) Su, H.-C.; Cheng, C.-Y. Recent Advances in Solid-State White Light-Emitting Electrochemical Cells. *Isr. J. Chem.* **2014**, *54*, 855−866.
(29) Kaihovirta, N.; Larsen, C.; Edman, L. Improving the Performance of Light-Emitting Electrochemical Cells by Optical Design. *ACS Appl. Mater. Interfaces* **2014**, *6*, 2940−2947.
(30) Lin, G.-R.; Chen, H.-F.; Shih, H.-C.; Hsu, J.-H.; Chang, Y.; Chiu, C.-H.; Cheng, C.-Y.; Yeh, Y.-S.; Su, H.-C.; Wong, K.-T. Non-Doped Solid-State White Light-Emitting Electrochemical Cells Employing the Microcavity Effect. *Phys. Chem. Chem. Phys.* **2015**, *17*, 6956−6962.
(31) Lindh, E. M.; Lundberg, P.; Lanz, T.; Edman, L. Optical Analysis of Light-Emitting Electrochemical Cells. *Sci. Rep.* **2019**, *9*, 10433.
(32) Dosso, J.; Tasseroul, J.; Fasano, F.; Marinelli, D.; Biot, N.; Fermi, A.; Bonifazi, D. Synthesis and Optoelectronic Properties of Hexa-Peri-Hexabenzoborazinocoronene. *Angew. Chem., Int. Ed.* **2017**, *56*, 4483−4487.
(33) Fresta, E.; Volpi, G.; Garino, C.; Barolo, C.; Costa, R. D. Contextualizing Yellow Light-Emitting Electrochemical Cells Based on a Blue-Emitting Imidazo-Pyridine Emitter. *Polyhedron* **2018**, *140*, 129−137.
(34) Aygüler, M. F.; Weber, M. D.; Puscher, B. M. D.; Medina, D. D.; Docampo, P.; Costa, R. D. Light-Emitting Electrochemical Cells Based on Hybrid Lead Halide Perovskite Nanoparticles. *J. Phys. Chem. C* **2015**, *119*, 12047−12054.
(35) Frohleiks, J.; Wepfer, S.; Kelestemur, Y.; Demir, H. V.; Bacher, G.; Nannen, E. Quantum Dot/Light-Emitting Electrochemical Cell Hybrid Device and Mechanism of Its Operation. *ACS Appl. Mater. Interfaces* **2016**, *8*, 24692−24698.
(36) Subeesh, M. S.; Shanmugasundaram, K.; Sunesh, C. D.; Chitumalla, R. K.; Jang, J.; Choe, Y. Host-Dopant System to Generate Bright Electroluminescence from Small Organic Molecule Functionalized Light-Emitting Electrochemical Cells. *J. Phys. Chem. C* **2016**, *120*, 12207−12217.
(37) Weber, M. D.; Fresta, E.; Elie, M.; Miehlich, M. E.; Renaud, J.-L.; Meyer, K.; Gaillard, S.; Costa, R. D. Rationalizing Fabrication and Design toward Highly Efficient and Stable Blue Light-Emitting Electrochemical Cells Based on NHC Copper(I) Complexes. *Adv. Funct. Mater.* **2018**, *28*, 1707423.
(38) Henwood, A. F.; Zysman-Colman, E. Luminescent Iridium Complexes Used in Light-Emitting Electrochemical Cells (LEECs). *Top. Curr. Chem.* **2016**, *374*, 36.
(39) Fresta, E.; Carbonell-Vilar, J. M.; Yu, J.; Armentano, D.; Cano, J.; Viciano-Chumillas, M.; Costa, R. D. Deciphering the Electroluminescence Behaviour of Silver (I)-Complexes in Light-Emitting Electrochemical Cells: Limitations and Solutions towards Highly Stable Devices. *Adv. Funct. Mater.* **2019**, *29*, 1901797.
(40) Fresta, E.; Volpi, G.; Milanesio, M.; Garino, C.; Barolo, C.; Costa, R. D. Novel Ligand and Device Designs for Stable Light-Emitting Electrochemical Cells Based on Heteroleptic Copper(I) Complexes. *Inorg. Chem.* **2018**, *57*, 10469−10479.
(41) Seyler, H.; Purushothaman, B.; Jones, D. J.; Holmes, A. B.; Wong, W. W. H. Hexa-Peri-Hexabenzocoronene in Organic Electronics. *Pure Appl. Chem.* **2012**, *84*, 1047−1067.
(42) Bonaccorso, F.; Sun, Z.; Hasan, T.; Ferrari, A. C. Graphene Photonics and Optoelectronics. *Nat. Photonics* **2010**, *4*, 611−622.
(43) Lundberg, P.; Lindh, E. M.; Tang, S.; Edman, L. Towards Efficient and Metal-Free Emissive Devices: A Solution-Processed Host-Guest Light-Emitting Electrochemical Cell Featuring Thermally Activated Delayed Fluorescence. *ACS Appl. Mater. Interfaces* **2017**, *9*, 28810−28816.
(44) Tang, S.; Tan, W.-Y.; Zhu, X.-H.; Edman, L. Small-Molecule Light-Emitting Electrochemical Cells: Evidence for in Situ Electrochemical Doping and Functional Operation. *Chem. Commun.* **2013**, *49*, 4926−4928.
(45) Shanmugasundaram, K.; Subeesh, M. S.; Sunesh, C. D.; Chitumalla, R. K.; Jang, J.; Choe, Y. Green Electroluminescence from Charged Phenothiazine Derivative. *J. Phys. Chem. C* **2016**, *120*, 20247−20253.
(46) Wong, M. Y.; Hedley, G. J.; Xie, G.; Kölln, L. S.; Samuel, I. D. W.; Pertegás, A.; Bolink, H. J.; Zysman-Colman, E. Light-Emitting Electrochemical Cells and Solution-Processed Organic Light-Emitting Diodes Using Small Molecule Organic Thermally Activated Delayed Fluorescence Emitters. *Chem. Mater.* **2015**, *27*, 6535−6542.
(47) Chen, H.-F.; Liao, C.-T.; Su, H.-C.; Yeh, Y.-S.; Wong, K.-T. Highly Efficient Exciplex Emission in Solid-State Light-Emitting Electrochemical Cells Based on Mixed Ionic Hole-Transport Triarylamine and Ionic Electron-Transport 1,3,5-Triazine Derivatives. *J. Mater. Chem. C* **2013**, *1*, 4647−4654.
(48) Bolink, H. J.; Cappelli, L.; Cheylan, S.; Coronado, E.; Costa, R. D.; Lardiés, N.; Nazeeruddin, M. K.; Ortí, E. Origin of the Large Spectral Shift in Electroluminescence in a Blue Light Emitting Cationic Iridium(III) Complex. *J. Mater. Chem.* **2007**, *17*, 5032−5041.
(49) Cho, Y. J.; Taylor, S.; Aziz, H. Increased Electromer Formation and Charge Trapping in Solution-Processed versus Vacuum-Deposited Small Molecule Host Materials of Organic Light-Emitting Devices. *ACS Appl. Mater. Interfaces* **2017**, *9*, 40564−40572.
(50) Yu, H.; Zhang, Y.; Cho, Y. J.; Aziz, H. Exciton-Induced Degradation of Carbazole-Based Host Materials and Its Role in the Electroluminescence Spectral Changes in Phosphorescent Organic Light Emitting Devices with Electrical Aging. *ACS Appl. Mater. Interfaces* **2017**, *9*, 14145−14152.
(51) Li, J. Y.; Liu, D.; Ma, C. W.; Lengyel, O.; Lee, C.-S.; Tung, C.-H.; Lee, S. T. White-Light Emission from a Single-Emitting-Component Organic Electroluminescent Device. *Adv. Mater.* **2004**, *16*, 1538−1541.
(52) Yang, S.; Jiang, M. White Light Generation Combining Emissions from Exciplex, Excimer and Electromer in TAPC-Based Organic Light-Emitting Diodes. *Chem. Phys. Lett.* **2009**, *484*, 54−58.
(53) Bastatas, L. D.; Lin, K.-Y.; Moore, M. D.; Suhr, K. J.; Bowler, M. H.; Shen, Y.; Holliday, B. J.; Slinker, J. D. Discerning the Impact of a Lithium Salt Additive in Thin-Film Light-Emitting Electrochemical Cells with Electrochemical Impedance Spectroscopy. *Langmuir* **2016**, *32*, 9468−9474.
(54) Puscher, B. M. D.; Aygüler, M. F.; Docampo, P.; Costa, R. D. Unveiling the Dynamic Processes in Hybrid Lead Bromide Perovskite Nanoparticle Thin Film Devices. *Adv. Energy Mater.* **2017**, *7*, 1602283.
(55) Bastatas, L. D.; Moore, M. D.; Slinker, J. D. The Effect of the Dielectric Constant and Ion Mobility in Light-Emitting Electrochemical Cells. *Chempluschem* **2018**, *83*, 266−273.
(56) Pershin, A.; Hall, D.; Lemaur, V.; Sancho-Garcia, J. C.; Muccioli, L.; Zysman-Colman, E.; Beljonne, D.; Olivier, Y. Highly Emissive Excitons with Reduced Exchange Energy in Thermally Activated Delayed Fluorescent Molecules. *Nat. Commun.* **2019**, *10*, 597.
(57) Fresta, E.; Costa, R. D. Advances and Challenges in White Light-Emitting Electrochemical Cells. *Adv. Funct. Mater.* **2020**, 1908176.
(58) Kaihovirta, N.; Asadpoordarvish, A.; Sandstro, A.; Edman, L. Doping-Induced Self-Absorption in Light-Emitting Electrochemical Cells. *ACS Photonics* **2014**, *1*, 182.